1   **ORIGINAL ARTICLE**

2

3   **During photosynthetic induction, biochemical and stomatal limitations differ between**

4   **Brassica crops**

5   Taylor, Samuel H.[1]*, Orr, Douglas J. [1], Carmo-Silva, Elizabete[1], and Long, Stephen P. [1,2]

6   [1]Lancaster Environment Centre, Lancaster University, Lancaster, LA1 4YQ, UK

7   [2]Departments of Plant Biology and of Crop Sciences, Carl R. Woese Institute of Genomic

8   Biology, University of Illinois, 1206 W. Gregory Dr., Urbana, IL 61801, USA

9   Running title: Photosynthetic induction in *Brassica* crops

10   *corresponding author: s.taylor19@lancaster.ac.uk

11

12   **Abstract**

13   Interventions to increase crop radiation use efficiency rely on understanding how biochemical

14   and stomatal limitations affect photosynthesis. When leaves transition from shade to high

15   light, slow increases in maximum Rubisco carboxylation rate and stomatal conductance limit

16   net CO_2 assimilation for several minutes. However, as stomata open, intercellular $[CO_2]$

17   increases, so electron transport rate could also become limiting. Photosynthetic limitations

18   were evaluated in three important *Brassica* crops: *B. rapa*, *B. oleracea* and *B. napus*.

19   Measurements of induction after a period of shade showed that net CO_2 assimilation by *B.*

20   *rapa* and *B. napus* saturated by 10 min. A new method of analyzing limitations to induction

21   by varying intercellular $[CO_2]$ showed this was due to co-limitation by Rubisco and electron

22   transport. By contrast, in *B. oleracea*, persistent Rubisco limitation meant that CO_2

23   assimilation was still recovering 15 min after induction. Correspondingly, *B. oleracea* had the

24   lowest Rubisco total activity. The methodology developed, and its application here, shows a

25   means to identify the basis of variation in photosynthetic efficiency in fluctuating light, which

26   could be exploited in breeding and bioengineering to improve crop productivity.

Introduction

The continued growth of the global human population and its increasing urbanisation will lead to increased pressure on farming systems over the next half century, and increased productivity on the land we are already using will be crucial to minimize the environmental impacts (Tilman, Balzer, Hill & Befort 2011). In this context, it is essential to understand photosynthetic efficiency because it fundamentally affects the productivity and efficiency of resource use by crops. The majority of crops use C_3 photosynthesis, which requires massive investment of nitrogen in leaf chloroplasts, where 21-74% of leaf soluble protein is allocated to the primary CO_2 fixing enzyme ribulose-1,5-bisphosphate (RuBP) carboxylase/oxygenase (Rubisco; Carmo-Silva, Scales, Madgwick & Parry 2015). Furthermore, A cost of allowing CO_2 into the leaf for photosynthesis, is the escape of water vapour via transpiration (Farquhar & Sharkey 1982; Raschke 1975). Consequently, crop biological N_2 fixation and crop applied N fertilisers now account for more than 44% of the total annual N entering the global biosphere (Fowler *et al*. 2013), and crop irrigation accounts for 70% of annual global human water use (Haddeland *et al.* 2014).

The major focus of studies of crop photosynthetic efficiency has been under light-saturating steady-state conditions. Yet these are rare for crop leaves in the field or glasshouse. Importantly, crop photosynthetic efficiency may be substantially affected by dynamic regulation in non-steady-state conditions. Adjustments to cope with changes in availability of light, e.g., caused by temporary shading within crop canopies, result in deviation from performance optima that are measured and defined in terms of steady-state conditions (Kaiser *et al*. 2016; Kromdijk *et al*. 2016; Lawson & Vialet-Chabrand, 2019; Morales *et al.* 2018; Tanaka, Adachi & Yamori, 2019; Taylor & Long 2017; Wang, Burgess, de Becker & Long 2020; Zhu, Ort, Whitmarsh & Long 2004). The effects of non-steady-state conditions on

55   photosynthetic efficiency, including the effects of temporary shade, remain poorly

56   characterised for a great many crop species.

57   Currently, a leading strategy for increasing crop efficiency is to improve radiation use

58   efficiency (Ort *et al.* 2015; Zhu, Long & Ort 2010). A key area of progress is improving the

59   speed at which photosynthesis responds to dynamic variation in sun and shade. Slow

60   relaxation of non-photochemical quenching (NPQ) during sun-shade transitions is one factor

61   that limits crop radiation use efficiency (Zhu *et al.* 2004), and speeding up this process has

62   been shown to increase plant productivity (Kromdijk *et al.* 2016). Slow induction of

63   photosynthesis during shade-sun transitions is also potentially important (Kaiser *et al.* 2015;

64   Pearcy, Krall & Sassenrath-Cole 1996). Evidence suggests that slow induction significantly

65   decreases diurnal CO_2 assimilation, and/or that there is significant genetic variation in rates of

66   induction amenable to breeding in wheat (Salter, Merchant, Richards, Trethowan & Buckley

67   2019; Taylor & Long 2017), rice (Acevedo-Siaca *et al.* 2020; Yamori, Masumoto, Fukayama

68   & Makino 2012), cassava (De Souza, Wang, Orr, Carmo-Silva & Long 2020), and soya

69   (Soleh *et al.* 2016; Wang *et al.* 2020). However, dynamic changes in the components of non-

70   stomatal limitations affecting photosynthesis during shade-sun transitions have been

71   characterised infrequently, so it remains unclear whether interventions that target specific

72   biochemical processes limiting induction of photosynthesis, e.g., increasing rates of Rubisco

73   activation (Yamori *et al.* 2012), will be similarly effective in a broad range of crop species.

74   For C_3 leaves, supply of CO_2 mediated by stomatal conductance (Farquhar &

75   Sharkey, 1982) results in net CO_2 assimilation rate (*A*)-intercellular [CO_2] (c_i) relationships

76   (A/c_i responses) that are expected to be controlled by different biochemical limitations

77   depending on c_i. At high light and lower c_i, photosynthesis is usually limited by maximum

78   rates of RuBP carboxylation by Rubisco ($V_{c,max}$), but above a threshold c_i ($c_{i, trans}$) RuBP

79   regeneration resulting from Calvin Benson Cycle turnover, driven principally by rates of

4

80   electron transport (J) becomes limiting (von Caemmerer & Farquhar 1981; Farquhar, von

81   Caemmerer & Berry, 1980). Robert Pearcy and colleagues first extended this model to

82   photosynthetic induction during the 1980s (reviewed in Pearcy *et al.* 1996), and their

83   dynamic A/c_i method (Chazdon & Pearcy, 1986) remains a gold standard for analysing

84   biochemical limitation during shade-sun transitions (Acevedo-Siaca *et al.* 2020; De Souza *et*

85   *al.* 2020; Salter *et al.* 2019; Soleh *et al.* 2016; Taylor & Long, 2017). The dynamic A/c_i

86   approach consists of a series of inductions measured at different $[CO_2]$s. Early applications

87   provided evidence that, subsequent to a 1-2 min RuBP-regeneration limited 'fast-phase'

88   (Sassenrath-Cole & Pearcy 1992), slow increases in both $V_{c,max}$ and g_s are key controls

89   affecting the rate at which A recovers following shade (Chazdon & Pearcy, 1986;

90   Kirschbaum & Pearcy, 1988). This understanding facilitated subsequent work addressing the

91   function of Rubisco activase (Rca), which drives increases in $V_{c,max}$ during induction (Carmo-

92   Silva & Salvucci, 2013; Hammond, Andrews, Mott & Woodrow 1998; Woodrow & Mott,

93   1989), and the assumption of persistent $V_{c,max}$ limitation during induction has recently been

94   used to improve methods for analysing biochemical and stomatal limitations during induction

95   (Deans, Farquhar & Busch 2019a).

96   Despite their importance, a caveat of published dynamic A/c_i measurements is

97   potential feedback between c_i and photosynthetic induction: greater c_i following shade is

98   linked with faster induction (Kaiser, Kromdijk, Harbinson, Heuvelink & Marcelis, 2017;

99   Kirschbaum & Pearcy 1988; Woodrow, Kelly & Mott 1996). Because this effect could inflate

100 apparent rates of increase in $V_{c,max}$ obtained from dynamic A/c_i experiments, and

101 underestimate absolute effects of $V_{c,max}$ on induction, alternative protocols that establish the

102 dynamic behaviour of $V_{c,max}$ without holding leaves at different $[CO_2]$s for extended periods

103 can better establish impacts on crop performance.

104   The [CO$_2$] denoting the transition from limitation by $V_{c,max}$ to limitation by J on the

105   A/c_i response ($c_{i,trans}$) is an important parameter for understanding photosynthetic efficiency.

106   Atmospheric [CO$_2$] is higher today than at any stage since domestication of crop plants began

107   (Indermühle $et\ al$. 1999; Larson $et\ al$. 2014; Sage 1995). Therefore, limitation by $V_{c,max}$

108   because of low c_i is likely to have been an important constraint on crop photosynthesis,

109   including photosynthetic induction, throughout the history of agriculture. Today and in the

110   future, however, higher ambient [CO$_2$] and/or increasing nitrogen limitation (which

111   diminishes $V_{c,max}$ and J) may result in more frequent limitation of A by J, including under

112   saturating light conditions where $V_{c,max}$ would previously have been the primary biochemical

113   control (Long, Ainsworth, Rogers & Ort 2004; Kromdijk & Long 2016). Whether the

114   operating point for A falls at, or towards higher or lower c_i than $c_{i,trans}$, will impact

115   photosynthetic optimisation and therefore efficiency of resource use under steady state

116   conditions. Photosynthesis at or close to $c_{i,trans}$ implies balanced Calvin Benson Cycle

117   function, maximizing returns on investment towards RuBP carboxylation and regeneration

118   capacity (von Cammerer & Farquhar, 1981; Farquhar & Sharkey, 1982; Long $et\ al$. 2004;

119   Kromdijk & Long 2016). Because the dynamic A/c_i method enables $c_{i,trans}$ to be determined

120   under non-steady-state conditions (Taylor & Long 2017) and establishes the patterns and

121   impacts of changes in V_{cmax} and J, dynamic A/c_i measurements can provide unique

122   mechanistic insights into deviations from optimal photosynthesis during induction.

123   Crops from the genus $Brassica$ (L.) are key sources of vitamins and minerals globally

124   (Rakow 2004) and provide interesting physiological contrasts. $Brassica$ can differ

125   considerably in terms of e.g., leaf size and thickness, and may be annual or biennial, which

126   would be expected to drive alternative leaf structural and biochemical investments (Wright et

127   al. 2004). The origins and inter-relationships between $Brassica$ species are well understood

128   (Liu $et\ al$. 2014; Parkin $et\ al$. 2005; Rana $et\ al$. 2004). From the perspective of understanding

129 how induction varies among crop accessions, the relationship between *B. oleracea* (L.)*, B.*

130 *rapa* (L.), and their allopolyploid hybrid *B. napus* (L.) is particularly interesting. Divergence

131 between *B. oleracea* and *B. rapa* occurred as much as 4 Mya (Inaba & Nishio 2002), and *B.*

132 *napus* most likely originated in agricultural settings, i.e., < 10 kya (Rana *et al.* 2004).

133 Consequently, gene families from both *B. oleracea* and *B. rapa* that are present in the

134 allopolyploid *B. napus* genome (Rana *et al*., 2004), may include those specifying the small

135 subunit of Rubisco and *Rca*. Their evolutionary history, therefore, makes these three species

136 an interesting test of the extent to which fairly close relatives can show differentiation in non-

137 steady-state photosynthesis, especially the impacts of $V_{c,max}$ on induction.

138   Using gas exchange and chlorophyll fluorescence, limitations affecting steady-state

139 and non-steady-state photosynthesis were determined for *B. oleracea*, *B. napus* and *B. rapa*.

140 1) Steady-state leaf gas exchange was used in combination with biochemistry of leaf extracts

141 to determine whether photosynthetic characteristics, including the predominant biochemical

142 limitation, differed. 2) Gas exchange time-series for induction measured at ambient $[CO_2]$

143 were used to establish whether there were differences in terms of: fast- (before 2 min) and

144 slow- (after 2 min) phases of induction, as well as periods dominated by non-stomatal factors,

145 which include biochemistry (decreasing c_i), or effects of increasing g_s (increasing c_i). 3)

146 Apparent biochemical limitations during induction were established in detail using a new

147 dynamic A/c_i response methodology, designed to overcome a key caveat of previous

148 experiments by not holding leaves at sub- or super-ambient $[CO_2]$s for extended periods.

149 **Materials and Methods**

150 *Plant material*

151 The three *Brassica* were represented by: a commercial winter oil seed rape, *B. napus* cv.

152 Elgar (Elsoms Seeds Ltd. Spalding, UK); Yellow Sarson, *B. rapa* ssp. *trilocularis* genotype

153   R-o-18, which has a similar developmental ontogeny to oilseed rape (Stephenson *et al.* 2010);

154   and Gai lan, *B. oleracea* ssp. *alboglabra*, genotype A12DHd (R-o-18 and A12DHd, Warwick

155   Crop Centre, Wellesbourne, UK).

156   Plants used for gas exchange measurements grew in controlled environment

157   greenhouses set to maintain day/night temperatures at 24/18 °C. A 16 h daylength was

158   maintained using supplementary lighting from high pressure sodium lamps (SON-T 400W,

159   Philips Lighting, Eindhoven NL) that provided a photosynthetic photon flux density (PPFD)

160   of ~ 500 μmol m^{-2} s^{-1} at canopy level if external short-wave irradiance decreased below 250

161   W m^{-2} (~ 570 μmol m^{-2} s^{-1} PPFD). Seedlings were germinated in 40 mL cells (PG Mix,

162   Yara, Grimsby, UK), and were transplanted to 1.5 L pots one week after emergence, in each

163   case using a soil-less compost mix (Petersfield Products, Leicester, UK) that incorporated a

164   broad range fertilizer. Checks were made daily to ensure that compost was kept moist without

165   overwatering.

166   Plants used for biochemistry were also sown, germinated and transplanted to 1.5 L

167   pots in the greenhouse, containing the same compost mix as above. They were then

168   transferred into controlled environment cabinets (Microclima 1750, Snijders Scientific B.V.,

169   Netherlands) two weeks after transplanting. Cabinets were set to maintain day/night

170   temperatures at 25/15 °C, RH was maintained at ~ 60%, and a 16 h daylength was achieved

171   with canopy-level PPFD ~ 450 μmol m^{-2} s^{-1}. Each species was sampled in five repeats of the

172   experiment: four plants per species were transferred to the controlled environment cabinet,

173   and after ~ 24 d in the cabinet, one leaf disc (0.55 cm^2) per plant was taken from the youngest

174   fully expanded leaf and immediately snap frozen in liquid N$_2$. To average out the effects of

175   plant-to-plant variation, within each of the five batches of plants, the four discs per species

176   were pooled for the Rubisco content and activity analyses described below.

Steady state photosynthesis

Measurements were made 5-6 weeks after planting for *B. rapa* and *B. napus*, and one or two weeks later for the slower growing *B. oleracea*. Recently expanded leaves were enclosed in the controlled environment cuvette of a photosynthesis system (LI-6800F, LI-COR, Lincoln NE, USA), which incorporates open-path infra-red CO_2 and H_2O analysers, and an integrated modulated fluorometer/light source. Leaf temperature was controlled at 25 °C, and leaf-air vapour pressure deficit (VPD_{leaf}) at 1.2 kPa. To measure photosynthetic responses to PPFD, leaves were brought to steady-state (stable *A* and stomatal conductance to water (g_{sw}) over 5 min) at a PPFD of 1500 µmol m^{-2} s^{-1} and [CO_2] of 392 ± 3.5 µmol mol^{-1} (mean ± sd; reference channel 430 µmol mol^{-1}). PPFD was then varied to supply 2000, 1800, 1500, 1200, 1000, 800, 600, 500, 400, 300, 250, 200, 150, 100, 50, and 0 µmol m^{-2} s^{-1} inside the cuvette. Measurements were taken as soon as *A* stabilised at each PPFD. Leaves were brought back to steady-state under the initial conditions, then the steady-state response of *A* to c_i was determined using measurements at different reference CO_2 concentrations: firstly, 430, 300, 200, 150, 100, 50, and ~ 0 µmol mol^{-1}, then, after return to steady state at 430 µmol mol^{-1}; 500, 600, 700, 900, 1000, and 1200 µmol mol^{-1}. In addition to gas exchange parameters calculated following von Caemmerer and Farquhar (1981), measurements during CO_2 response curves captured steady state (F_s) and maximum (F_m') fluorescence yields using a multiphase flash, allowing use of the effective quantum yield [$\Phi_{PSII} = (F_m' - F_s)/F_m'$] as an additional indicator of photosynthetic limitation-state based on its proportionality with *J* (e.g., Gu *et al*. 2010, Busch & Sage 2017; Supplementary Fig. 1).

Photosynthetic induction

Photosynthetic induction responses at ambient [CO_2] were measured by establishing steady-state gas exchange at: PPFD, 1500 µmol m^{-2} s^{-1}; reference [CO_2], 430 µmol mol^{-1}; cuvette

201   air temperature, 25 °C; and cuvette RH 65% (VPD_{leaf} 1.08 ± 0.075 kPa). A shade fleck was

202   then simulated by a step decrease in PPFD to 150 µmol m^{-2} s^{-1} for 30 min, followed by a step

203   increase back to 1500 µmol m^{-2} s^{-1}. Gas analysers were matched one minute before starting

204   the sun-shade-sun sequence, and measurements were logged every 10 s from one min before

205   shade until at least 28 min after shade.

206   The following key timesteps from the 10 s resolution induction curves were

207   identified. First, the end of the RuBP regeneration dominated 'fast-phase' of induction was

208   taken to be 2 min after the return to high light, following shade. Second, $t_{ci,min}$ was the time at

209   which minimum c_i was observed during induction, marking the transition between

210   predominant limitation by non-stomatal factors (which results in decreasing c_i) and increasing

211   stomatal conductance (g_s; which results in increasing c_i). Next, $t_{A,90}$ was the timepoint at

212   which A had recovered 90% of the difference [A pre-shade – A end shade]. Using these

213   timepoints, recovery in A, as a proportion of [A pre-shade – A shade], was attributed to the

214   fast-phase (R_{fast}), non-stomatal dominated ($R_{ci,min}$), and non-stomatal dominated recovery not

215   attributable to the fast-phase ($R_{ci,min} - R_{fast}$), i.e., slow phase non-stomatal recovery. The

216   duration of recovery dominated by effects of g_s was approximated by $t_{A,90} - t_{ci,min}$.

217   *Dynamic A/c_i measurements*

218   To characterise changes in factors limiting photosynthesis during shade-sun transitions, a

219   dynamic A/c_i method was implemented that improved on previously published versions

220   (Acevedo-Siaca *et al*. 2020; Chazdon & Pearcy 1986; De Souza *et al*. 2020; Salter *et al.*

221   2019; Soleh *et al*. 2016; Taylor & Long 2017) by removing the potentially confounding

222   effect of extended incubation in various [CO_2]s. Leaves were first brought to steady state

223   under the same conditions as for measurements of photosynthetic induction described above.

224   A 30 min period of shade was then imposed using a PPFD of 100 µmol m^{-2} s^{-1}. Following

225   Taylor & Long (2017), to prevent stomatal closure in response to this shade by maintaining c_i

226   at approximately twice the compensation point (spot measurements prior to end of shade

227   period: mean ± sd, 93 ± 1.3 μmol mol^{-1}, N = 328 inductions), reference [CO_2] was controlled

228   at 100 μmol mol^{-1} during the shade. At the end of 30 min shade, PPFD was returned to its

229   initial value of 1500 μmol m^{-2} s^{-1} and [CO_2] was set to the first of a stratified random

230   sequence of ten [CO_2]s, measured at two min intervals so that chamber stability and IRGA

231   matching could be achieved reliably. For each leaf to be measured, an independent sequence

232   of reference [CO_2]s was drawn from the following set: 50, 100, 200, 300, 400, 500, 600, 700,

233   800, and 1000 μmol mol^{-1}. The [CO_2]s were ordered so that concentrations from the ≤ 400

234   μmol mol^{-1} and ≥ 500 μmol mol^{-1} ranges were interspersed randomly (e.g., 800, 200, 600,

235   100, 500, 400, 700, 300, 1000, 50), and were rotated over ten separate inductions so that

236   every [CO_2] was measured at every interval between 2 and 20 min following shade

237   (Supplementary Fig. 2). To aid with consistency of responses, measurements were made in

238   the laboratory (i.e., low light, and relatively constant temperature and humidity conditions),

239   and between inductions gas exchange was allowed to fully recover to steady state at reference

240   [CO_2] of 430 μmol mol^{-1}. To ensure that induction measurements for a leaf could be captured

241   within a single day, two LI-6800F were used, attached adjacent to one another, either side of

242   the mid-rib.

243   *Models*

244   The relationship between *A* and incident PPFD was modelled as a non-rectangular hyperbola

245   (Long & Hallgren 1985):

246

$$A = \frac{\phi I + A_{\text{sat}} - \sqrt{(\phi I + A_{\text{sat}})^2 - 4\theta\phi I A_{\text{sat}}}}{2\theta} - R_{\text{d}}$$

247 Where: ϕ is the apparent quantum yield (mol mol^{-1}); I, incident PPFD (µmol m^{-2} s^{-1}); A_{sat},

248 the maximum gross rate of leaf CO_2 assimilation (µmol m^{-2} s^{-1}); θ, a dimensionless curvature

249 parameter; and R_d, day respiration (µmol m^{-2} s^{-1}).

250 With values for [CO_2] in partial pressure units, the FvCB model (von Caemmerer &

251 Farquhar 1981; Farquhar *et al*. 1980) was used to characterise A/c_i relationships:

$$A = min(W_C, W_J, W_P)(1 - \Gamma^*/c_c) - R_d$$

$$W_C = V_{c,max}c_c/(c_c + K_{CO})$$

$$W_J = Jc_c/(4c_c + 8\Gamma^*)$$

$$W_P = 3T_P c_c/(c_c - \Gamma^*)$$

256 where W_C is the Rubisco limited, W_J electron transport limited, and W_P triose-phosphate

257 utilisation limited rate of carboxylation. The [CO_2] at the site of carboxylation in the

258 chloroplast, $c_c = c_i - A/g_m$. Additional parameters are: Γ^*, the photosynthetic CO_2

259 compensation point in the absence of R_d; $V_{c,max}$, the maximum carboxylation rate of Rubisco;

260 $K_{CO} = K_C(1+O/K_O)$, where K_C and K_O are the respective Michaelis constants for Rubisco

261 catalysis of carboxylation and oxygenation reactions, and O is the partial pressure of O_2; J,

262 electron transport rate; T_P, the rate of triose phosphate utilisation.

263 To identify the match between c_i and W_C, W_J, and W_P as limiting factors we used the

264 approach of Gu, Pallardy, Tu, Law & Wullschleger (2010), fitting values for $V_{c,max}$, J, and T_P

265 using:

$$A = \frac{b - \sqrt{b^2 - 4c}}{2}$$

267 For A_C:

$$b = V_{c,max} - R_d + g_m(c_i + K_{CO})$$

$$c = g_m \left(V_{c,max}(c_i - \Gamma^*) - R_d(c_i + K_{CO}) \right)$$

270 For A_J:

12

271
$$b = J/4 - R_d + g_m(c_i + 2\Gamma^*)$$

272
$$c = g_m\big(J/4(c_i - \Gamma^*) - R_d(c_i + 2\Gamma^*)\big)$$

273 For A_P:

274
$$b = 3T_p - R_d + g_m(c_i - \Gamma^*)$$

275
$$c = g_m\big(3T_P(c_i - \Gamma^*) - R_d(c_i - \Gamma^*)\big)$$

276   For each A/c_i response, all possible limitation-state combinations were tested, given

277 the required order of limitation states along the c_i axis ($W_C < W_J < W_P$), and the minimum

278 number of data necessary for each limitation state (N $\geq$ 2 when K_{CO} and Γ^* are fixed). The R

279 Language and Environment function *optim* (R Core Team 2018) was used to minimise the

280 distribution-wise cost function, accepting the model with the lowest value after checking for

281 admissibility and testing for co-limited 'swinging points' (Gu *et al.* 2010).

282   Using this method, estimation of g_m from the data was found not to credibly predict

283 limitation states indicated by Φ_{PSII} (e.g., Busch & Sage 2017), so for consistency g_m was

284 assumed to be infinite throughout (approximated by setting g_m to 1×10^6 µmol m^{-2} s^{-1} Pa^{-1}).

285 Values for $V_{c,max}$, J and T_P are thus apparent rates, and in the dynamic A/c_i analysis are

286 confounded with any dynamic variation in g_m. Similarly, to ensure credible values, mean leaf

287 temperatures measured in the LI-6800F were used to predict Γ^*, K_C and K_O, using values for

288 tobacco (Sharkey, Bernacchi, Farquhar & Singsaas 2007). Combining the Sharkey *et al.*

289 (2007) coefficients with estimation of R_d as part of the fitting process provided the best fit in

290 the region around Γ^* for parameterisation of steady-state responses (for comparisons among

291 parameterisations, see Supplementary Fig. 3).

292   In the dynamic A/c_i analysis, where greater measurement error and a slightly reduced

293 number of measurements made least-squares fits less reliable, genotype-level parameters

294 from the steady-state A/c_i measurements were used to ensure A/c_i fits provided a reasonably

295 close match with limitation states indicated by Φ_{PSII} (Supplementary Fig. 2). The value of R_d

296   was fixed. In addition, A_p was initially assigned only to points with $c_i \geq$ that at which

297   limitation transitioned from J to T_p in the steady-state. If best-fit, admissible models predicted

298   T_p, they were only accepted if they also predicted $V_{c,max}$ and J, otherwise data assigned to A_P

299   were dropped and the model was refit, dropping the highest c_i data as necessary until a best-

300   fit admissible model was found that either (a) included both A_C and A_J, or (b) included A_C

301   alone. When a best fit model with A_C alone was reached, because identification of A_J requires

302   N $\geq$ 2, the uppermost c_i value was dropped to prevent mis-attribution of data that could be

303   assigned to A_J and the model was refit, taking the highest c_i used as a lower-bound value for

304    $c_{i,trans}$.

305   Stomatal limitation (L_S) was calculated from the steady-state A/c_i responses following

306   Farquhar & Sharkey (1982):

$$L_S = \frac{A_0 - A}{A_0}$$

307

308   Where, A_0 is a reference net CO_2 assimilation rate predicted at a c_i equal to leaf external

309   [CO_2], and A was the rate observed at the initial reference [CO_2] of 430 μmol mol^{-1}.

310   *Analyses of Rubisco activity, and content of Rubisco, total soluble protein, and chlorophylls*

311   Leaf samples consisting of four leaf discs (2.2 cm^2 per sample) were homogenised in 0.6 mL

312   of extraction buffer (50 mM Bicine-NaOH pH 8.2, 20 mM MgCl$_2$, 1 mM EDTA, 2 mM

313   benzamidine, 5 mM ε-aminocaproic acid, 50 mM 2-mercaptoethanol, 10 mM dithiothreitol,

314   1% (v/v) protease inhibitor cocktail (Sigma-Aldrich, Mo, USA), and 1 mM

315   phenylmethylsulphonyl fluoride) using an ice-cold mortar and pestle. Rapid grinding (< 60 s)

316   was followed by centrifugation of the homogenate at 4 °C, 21000 g for 1 min. The

317   supernatant was collected and used to determine Rubisco total activity by $^{14}CO_2$

318   incorporation into acid-stable products as described previously (Carmo-Silva *et al.* 2017).

319   The supernatant (20 mm^3) was incubated for 3 min in 500 mm^3 of reaction mixture (100 mM

14

320 Bicine-NaOH pH 8.2, 20 mM MgCl$_2$, 10 mM NaH^{14}CO$_2$ [9.25 kBq umol^{-1}], and 2 mM

321 KH$_2$PO$_4$) to fully carbamylate Rubisco. RuBP was then added (to 0.6 mM) to initiate the

322 reaction, and assays quenched with 10 M formic acid after 30 s. Reaction mixtures were

323 dried, the residue re-suspended, and scintillation counted as described previously (De Souza,

324 *et al*. 2020). The same supernatant was used to determine Rubisco content by mixing 100

325 mm^3 of supernatant with 100 mm^3 of CABP binding buffer (100 mM Bicine-NaOH pH 8.2,

326 20 mM MgCl$_2$, 20 mM NaHCO$_3$, 1.2 mM [^{14}C]CABP [carboxyarabinitol-1,5-bisphosphate,

327 37 kBq µmol^{-1}]), incubating at ~ 20 °C for 30 min, then following the column-based

328 [^{14}C]CABP binding assay described previously (Sharwood, Sonawane, Ghannoum &

329 Whitney 2016).

330   Total soluble protein (TSP) was determined for aliquots taken from the supernatant

331 used for Rubisco analyses via Bradford assay (Bradford 1976). Chlorophyll content was

332 determined from an aliquot of the leaf homogenates prior to centrifugation, which was added

333 to ethanol (Wintermans & de Mots 1965). Absorbance for TSP and chlorophyll

334 determinations was measured in a SPECTROstar Nano microplate reader (BMG LabTech,

335 Aylesbury, UK).

336 *Statistical analyses*

337 Modelling and statistical analyses were carried out using R Language and Environment 3.5.2

338 (R Core Team 2018). Among species differences were tested using one-way anova and

339 Tukey's Honest Significant Difference, and the homogeneity assumption was validated using

340 Bartlett's test.

341   For parameters from dynamic A/c_i analysis, generalised additive mixed models

342 (GAMM, package *mgcv* version 1.8-26) were used to summarize time-dependent changes

343 without the need to assume particular underlying mechanisms. When fitting GAMM,

15

344   *Brassica* species were treated as fixed effects, allowing unique species-level functions with

345   respect to time. Independently measured plants were treated as random effects influencing

346   variance around the species-level functions (Zuur, Ieno, Walker, Saveliev & G M Smith

347   2009). The slopes of fitted functions for $V_{c,max}$ against time ($dV_{c,max}/dt$) from dynamic A/c_i

348   were obtained by finite differencing from values predicted by GAMM at 1 s resolution.

349   Species specific confidence intervals for GAMM were approximated as: predicted values ±

350    $t_{1-\alpha,edf} \times$ SEM, where $\alpha = 0.025$, and edf = estimated degrees of freedom at the species level.

351   **Results**

352   ***Steady state photosynthesis and biochemical characteristics***

353   *Photosynthetic response to light and leaf biochemistry*

354   Leaf level responses to PPFD (Fig. 1) showed mean values of A_{sat} R_d, and θ that were highest

355   for *B. rapa*, slightly lower for *B. napus*, and lowest for *B. oleracea* (Fig. 1). By contrast, ϕ

356   was greater in *B. oleracea* and *B. napus* than in *B. rapa*. There was limited support for

357   significant differences in R_d ($F_{2,9} = 2.22$, P = 0.16) and ϕ ($F_{2,9} = 2.56$, P = 0.13) across the

358   three *Brassica*. However, differences in A_{sat} were marginally significant ($F_{2,9} = 3.03$, P =

359   0.099), and there was strong evidence for a significant difference in θ ($F_{2,9} = 9.91$, P = 0.005).

360   The smaller θ for *B. oleracea* compared with *B. napus* and *B. rapa*, supports a more gradual

361   transition from light- to carboxylation-limited photosynthesis at higher PPFDs and was

362   significant for both individual comparisons (P ≤ 0.026).

363   The observed patterns of differences in mean Rubisco total activity and Rubisco

364   amount were consistent with marginally significant differences in mean A_{sat}. Rubisco amount

365   and total activity were lower in *B. oleracea* than in *B. napus* and *B. rapa* (Table 1), though

366   these differences were not significant among the three species ($F_{2,12} \leq 1.6$, P ≥ 0.24).

367   Normalised to Rubisco content, Rubisco specific activities were even more similar than total

368　activities among the three *Brassica* (Table 1), implying that patterns of difference in total

369　activity were strongly affected by amounts of Rubisco protein per unit leaf area. Interestingly,

370　while the lower Rubisco content of *B. oleracea* leaves was paired with similar total soluble

371　protein to *B. rapa* (P = 0.94), these two species showed marked differences in chlorophylls.

372　*B. oleracea* had approximately double the amount of chlorophyll a+b (P < 0.001), and lower

373　chlorophyll a:b ratios (P = 0.001) compared with *B. rapa* (Table 1). By contrast, *B. napus* had

374　higher soluble protein content compared with the other two *Brassica* (P ≤ 0.029; Table 1),

375　intermediate chlorophyll content (*B. napus-B. oleracea,* P = 0.084; *B. napus-B. rapa,* P =

376　0.002) and intermediate chlorophyll a:b ratio (*B. napus-B. oleracea,* P = 0.089; *B. napus-B.*

377　*rapa,* P = 0.089). Thus, while Rubisco content was aligned with A_{sat}, it was opposite to

378　investments in chlorophyll pigments, which were significantly less in leaves of *B. rapa*

379　compared with *B. oleracea*.

380　*Photosynthetic response to CO_2*

381　Operating point *A* and g_{sw} were significantly lower for *B. oleracea* than for *B. rapa* (*A*, P =

382　0.021; g_{sw}, P = 0.017). For both *A* and g_{sw}, *B. napus* was intermediate between the other

383　*Brassica*: there was a marginally significant difference in *A* between *B. napus* and *B.*

384　*oleracea* (P = 0.064); little support for a significant difference in g_{sw} between them (P =

385　0.15); and no significant difference in either *A* or g_{sw} between *B. napus* and *B. rapa* (P ≥ 0.31;

386　Table 2). The significant differences between *A* and g_{sw} of *B. oleracea* and *B. rapa* were

387　associated with an increase in mean c_i from 26.5 (*B. oleracea*) to 29.3 Pa (*B. rapa*), but

388　measurements were not sufficiently repeatable across the small number of replicates to

389　establish a significant difference in c_i among the three species ($F_{2,9}$ = 2.56, P = 0.13; Table 1).

390　　　　The similarity in operating c_i, and differences in *A* and g_{sw} between the *Brassica* were

391　associated with differences in steady state A/c_i responses (Fig. 2; Supplementary Fig. 1).

17

392 Mean $V_{c,max}$ and J were, as for A, highest in *B. rapa*, intermediate in *B. napus*, and lowest in

393 *B. oleracea*. While the three primary rate limiting factors: $V_{c,max}$, J and T_P, were not

394 significantly different between the three *Brassica* ($F_{2,9} \leq 2.16$, $P \geq 0.17$; Fig. 2), differences in

395 L_S were ($F_{2,9} = 5.01$, $P = 0.035$), specifically between *B. rapa* and *B. oleracea* ($P = 0.037$,

396 other comparisons $P \geq 0.089$; Table 2). There was also a marginally significant difference in

397 $c_{i,trans}$ ($F_{2,9} = 4.1$, $P = 0.054$), with *B.oleracea* showing the highest $c_{i,trans}$ and *B.rapa* the

398 lowest: the range of c_i that is expected to result in $V_{c,max}$ limiting A was significantly greater

399 for *B. oleracea* than *B. rapa*. In combination, small differences in $V_{c,max}$, J, and g_s led to

400 operating c_i that was significantly lower than $c_{i,trans}$ in *B. oleracea* (one tailed, paired t-test: t_3

401 $= 3.61$, $P = 0.005$), but overlapped with $c_{i,trans}$ in *B. napus* and *B. rapa* (two tailed, paired t-

402 test: $t_3 < \pm 1.69$, $P \geq 0.19$). Thus, in the steady state, carboxylation in leaves of *B. oleracea*

403 was limited by $V_{c,max}$, whereas *B. napus* and *B. rapa* operated at the transition between $V_{c,max}$

404 and J limitation (Fig. 2; Supplementary Fig. 1). Finally, though at much higher c_i than the

405 operating point, a highly significant difference was also shown for the c_i at which A_J

406 transitioned to A_P ($F_{2,9} = 10.38$, $P = 0.006$), between *B napus*, which had the lowest value for

407 the c_i of this transition, and *B. oleracea,* which had the highest (Fig. 2; $P = 0.005$).

408 ***Photosynthetic induction***

409 *Recovery of A during fast, mesophyll-dominated, and stomata-limited induction*

410 The vast majority of recovery in A occurred while c_i was decreasing, i.e., while recovery of A

411 was controlled primarily by non-stomatal factors (Fig. 3); recovery of A during this 4-5 min

412 period ($t_{ci,min}$, Table 3) averaged 77-84% ($R_{ci,min}$, Table 3). After 30 min shade at the

413 relatively high shade-irradiance of 150 μmol m^{-2} s^{-1}, ~ 70% of recovery occurred during the

414 first 2 min (fast-phase), so slow-phase recovery prior to increases in c_i accounted for ~ 10%

415 of the shade-sun difference in A (Table 3). When the fast- and slow-phase components of

18

416   non-stomatal-dominated recovery were taken together, neither their combined impact on

417   recovery of A nor their combined duration were significantly different between the three

418   *Brassica* ($R_{ci,min}$, P = 0.51; $t_{ci,min}$, P = 0.24).

419   By contrast with non-stomatal-dominated induction, the remaining 20% of recovery

420   in A, that was predominated by the effect of increasing g_s on c_i, took significantly longer in *B.*

421   *oleracea* than in *B. rapa* ($t_{A,90} - t_{ci,min}$, Table 3; P = 0.02), and was marginally significantly

422   longer in *B. oleracea* than *B. napus* (Tukey HSD, P = 0.055; Table 3). Mean A, g_{sw} and c_i of

423   *B. oleracea* had not approached their steady-state values even after 20 min of induction (Fig.

424   4a), such that $t_{A,90}$ was significantly longer in *B. oleracea* than the other two species (Table 3;

425    $F_{2,9}$ = 7.24, P = 0.013; *B. oleracea-B.napus*, P = 0.034; *B. oleracea-B. rapa*, P = 0.017).

426   Contrasting with *B. oleracea*, both *B. napus* and *B. rapa* reached $t_{A,90}$ within 10 min

427   induction (Table 3), even though, like *B. oleracea*, their g_{sw} and c_i continued to increase

428   beyond 20 min, A was insensitive to this (Fig. 3 and 5).

429   *Apparent limiting biochemical factors during induction - dynamic A/c_i*

430   Progressive changes in $V_{c,max}$ determined from dynamic A/c_i responses were qualitatively

431   different between the three *Brassica* (Fig. 4). Increases in $V_{c,max}$ during induction were: 23%

432   in *B. oleracea*, 33% in *B.napus* and 29% in *B. rapa*. The rate of change in $V_{c,max}$ ($dV_{c,max}/dt$)

433   declined smoothly (Fig. 4d), and confirmed that increases in $V_{c,max}$ were predominantly over

434   the first ~ 10 min of induction in *B. oleracea* , ~ 12 min in *B. rapa* (Fig. 4a, c & d), and ~18

435   min in *B. napus* (Fig. 4b & d). In all three, $V_{c,max}$ increased rapidly for the first 4-5 min of

436   induction, coinciding with the $t_{ci,min}$ observed in induction measurements (Table 3). It was

437   also notable that $V_{c,max}$ of *B. oleracea* saturated before $t_{A,90}$ from the ambient induction

438   experiments, whereas increases in $V_{c,max}$ of *B. napus* and *B. rapa* were continuing at their

439    $t_{A,90}$, but with little subsequent effect on A (Fig. 4).

440   The c_i at which limitation transitioned away from $V_{c,max}$ ($c_{i,trans}$), which is co-

441   determined by $V_{c,max}$ and J, was initially similar to ambient [CO_2] and decreased during

442   induction. After 4-6 min induction, $c_{i,trans}$ was indistinguishable from steady-state values on

443   the basis of approximate 95% confidence intervals (Fig. 5). Comparing time series for $c_{i,trans}$

444   (shade PPFD, 100 μmol mol^{-1}) with c_i during induction at ambient [CO_2] (shade PPFD 150

445   μmol m^{-2} s^{-1}; Fig. 5), by 20 min their values were essentially the same as those found at

446   steady-state (i.e. *B. oleracea*, $c_i < c_{i,trans}$; *B. napus*, $c_i \sim c_{i,trans}$; *B. rapa* $c_i \sim c_{i,trans}$). Based on

447   95% confidence intervals, c_i was significantly less than $c_{i,trans}$ throughout induction for *B.*

448   *oleracea* (Fig. 5a), until $\sim$ 10 min for *B. napus* (Fig. 5b), and until $\sim$ 7 min in *B. rapa* (Fig.

449   5c), with c_i intersecting mean $c_{i,trans}$ after 10-15 min induction in *B. napus* and *B. rapa*.

450   Because $c_i < c_{i,trans}$ infers that A is limited by $V_{c,max}$, as $c_i < c_{i,trans}$ throughout induction A of *B.*

451   *oleracea* was always $V_{c,max}$-limited, and the other two species were $V_{c,max}$ limited beyond $t_{A,90}$

452   (Table 3). Because $c_{i,trans}$ denotes a change in the slope of the A/c_i response, overlap between

453    $c_{i,trans}$ and c_i of *B. napus* and *B. rapa* during induction explains why A saturated while their g_s

454   and c_i continued to increase (Fig 3b & c).

455   **Discussion**

456   Photosynthesis differed in several ways between *B. rapa* and *B. oleracea*. Most notably, the

457   former had greater rates of gas exchange and recovered steady-state A more rapidly following

458   shade. *B. napus* was intermediate in most respects, although more similar to *B. rapa*. A novel

459   dynamic A/c_i response protocol that added randomisation of [CO_2]s during induction to a

460   previous innovation of fixed low [CO_2] during shade (Taylor & Long 2017), imposed robust

461   control for [CO_2] during induction. The dynamic A/c_i experiments demonstrated that all three

462   *Brassica* were limited by apparent $V_{c,max}$ for 10 min or more following 30 min shade.

463   Importantly though, while *B. oleracea* stayed $V_{c,max}$ limited, *B. napus* and *B. rapa* transitioned

464 to co-limitation by J after ~ 10 min. The transitions to co-limitation coincided broadly with

465 saturation of A, explaining why ongoing increases in g_s and/or $V_{c,max}$ had little subsequent

466 effect in these two species, and providing a potential mechanistic explanation for previous

467 observations of diversity among species in rates of recovery of A relative to g_s (Deans,

468 Brodribb, Busch & Farquhar 2019b; McAusland *et al.* 2016).

469 *Limitations affecting steady-state photosynthesis*

470 The difference in limitation-states affecting steady-state A of the three species was not an

471 anticipated outcome, but was clear. All three operated within 5 Pa of their $c_{i,trans}$. This is

472 consistent with the hypothesis that operation close to $c_{i,trans}$ reflects optimisation of resource

473 investment between capacities for carboxylation and RuBP regeneration (von Caemmerer &

474 Farquhar 1981; Farquhar & Sharkey 1982), and perhaps indicative of acclimation to recent

475 rapid increases in atmonspheric [CO_2] (Long *et al*. 2004; Kromdijk & Long 2016).

476   The amount of Rubisco and its total activity were a match for species differences in

477 apparent $V_{c,max}$ and a better explanation of V_{cmax} than differences in Rubisco performance. All

478 three *Brassica* had similar Rubisco specific activities. Compared with Rubisco properties,

479 differences in chlorophyll and total soluble protein were more easily detected. *B. oleracea*

480 had double the chlorophyll a+b content compared with *B. rapa*, and the leaves of *B. oleracea*

481 showed a more gradual transition away from light limitation as PPFD increased (significantly

482 lower θ). *B. oleracea* A12DHd had particularly thick, noticeably waxy leaves and may

483 experience limited light saturation deeper in the mesophyll (Hikosaka & Terashima 1995),

484 especially when using the red/blue light source of the LI-6800F (Terashima *et al*. 2009).

485 Reflectance from the waxy leaf surface may also reduce absorption by *B. oleracea* leaves and

486 the species had lower chlorophyll a:b indicating a greater proportion of light harvesting

487 chlorophylls, consistent with shade adaptation within the leaf. Evidence from biochemistry

488   and light response curves is therefore consistent with linkages between different steady-state

489   photosynthetic limitations in these *Brassica* and higher-level structural differences.

490   Limitation of *A* by apparent $V_{c,max}$ in *B. oleracea* was clearly linked with lower g_s and

491   greater L_S than in *B. napus* and *B. rapa*. The other key component of diffusive limitation

492   affecting photosynthesis, g_m, was not reliably estimated with our data using exhaustive dual

493   optimisation. To obtain consistent visual matching between predicted limitation states and the

494   inflexion of both A/c_i and Φ_{PSII} in our three-species dataset required an effectively infinite

495   value for g_m. However, the modified exhaustive dual optimisation approach (Gu *et al*. 2010)

496   is a powerful tool for identifying $c_{i,trans}$ based on the inflexion of the A/c_i response, and

497   incorporating a finite value for g_m in the model of photosynthesis does not affect whether

498   operating point *A* falls above or below this inflexion.

499   Adequate fits for A/c_i responses in the region of Γ^* were achieved using the tobacco-

500   derived parameterisation of Sharkey *et al*. (2007). By contrast, estimates of Rubisco kinetic

501   parameters for *B. oleracea* reported in the literature (Hermida-Carrera, Kapralov & Galmés

502   2016) provided poor fits in this region (Supplementary Fig. 3). Compared with coefficients

503   based on gas exchange measurements using tobacco (Sharkey *et al*. 2007), values for *B.*

504   *oleracea* determined using *in vitro* measurements (Hermida-Carrera *et al*. 2016) are 7.5 Pa

505   less for K_{CO}, and 0.8 Pa greater for Γ^*. As a consequence, Rubisco kinetic properties from

506   Hermida-Carrera *et al*. (2016) predicted $V_{c,max}$ to be ~ 6% greater; however, their Γ^*

507   exceeded the CO_2 compensation points we measured in all three *Brassica* (Supplementary

508   Fig. 3). While the parameterisation we used for g_m means that the reported biochemical rates

509   of $V_{c,max}$ and *J* incorporate differences in mesophyll properties, the fact that total activity of

510   Rubisco from leaf extracts scaled with values for $V_{c,max}$ strongly corroborates the finding of

511   lower $V_{c,max}$ in *B. oleracea*. Irrespective of the differences between published kinetic

512   coefficients, therefore, *B. oleracea* had lower $V_{c,max}$ and was $V_{c,max}$ limited over a greater

513   range of c_i than the other two species. Increasing Rubisco activity (e.g., Salesse-Smith,

514   Sharwood, Busch, Kromdijk, Bardal & Stern 2018; Yoon *et al*. 2020) could be particularly

515   useful for improvement of photosynthesis in *B. oleracea,* assuming the genotype tested here

516   is representative of the species.

517   *Components of recovery in A during induction.*

518   In all three *Brassica*, in addition to 70% of recovery attributable to fast-phase RuBP

519   regeneration, and prior to increases in c_i and *A* linked with increasing g_s, slow-phase

520   induction was initially dominated by non-stomatal effects consistent with Rubisco activation,

521   which accounted for at least 10% of recovery in *A*. This fairly small value probably arose

522   because of the relatively high PPFD (150 μmol m^{-2} s^{-1}) used during shade, and the fact that

523   steady-state g_s was obtained in saturating light prior to imposing shade, hence relatively high

524   g_s at the start of induction (Kirschbaum & Pearcy 1988). Use of relatively high shade PPFD

525   and pre-acclimation to saturating light makes our measurements most relevant to midday

526   photosynthesis in upper layers of crop canopies (Burgess *et al*. 2016; Townsend *et al.* 2018;

527   Zhu *et al*. 2004). In situations where initial $V_{c,max}$ and/or g_s are lower, e.g., deeper layers of

528   crop canopies where sunlit periods are interspersed by longer shade periods or preceded by

529   persistent low light, more extended and larger impacts of $V_{c,max}$ would be expected when

530   leaves are sunlit (Morales *et al*. 2018). The relatively high PPFD used here during shade also

531   ensured that stomata remained the predominant route of water loss throughout our

532   experiments, decreasing the risk of errors in calculated c_i (Hanson, Stutz & Boyer 2016) and

533   enabling use of c_i as a sensitive indicator of whether mesophyll or diffusive factors were the

534   predominant control over *A*.

535   The initial decrease in c_i always extended to $\sim$ 4-5 min of induction, at least twice the

536   2 min assumed to mark the end of the RuBP-regeneration dominated fast-phase. The 2 min

537 upper limit for the fast-phase is taken from the literature (e.g., Sassenrath-Cole & Pearcy

538 1992), and was used because gas exchange system mixing times meant that fast-phase

539 kinetics could not be directly parameterised. The inflection of A indicating the end of the fast

540 phase nonetheless tended to occur slightly before 2 min (e.g., Fig. 3), so the estimate of

541 photosynthetic recovery driven by Rubisco activation, at 2-3 min duration and 10%, is

542 conservative. Evidence that shade-induced Rubisco deactivation can limit midday

543 photosynthesis in field crops is consistent with previous detailed measurements of apparent

544 $V_{c,max}$ following sun-shade-sun transitions in wheat (Taylor & Long 2017; Salter *et al*. 2019),

545 and experiments that manipulated *Rca* in rice (Yamori *et al*. 2012).

546   Beginning after 4-5 min of induction, increasing g_s outweighed non-stomatal

547 components as a determinant of increasing c_i and A. At this time $c_{i,trans}$ was very close to its

548 steady-state value. Despite the similar timing of transitions to g_s-dominated induction,

549 recovery in A was less strongly and persistently affected by g_s in *B. napus* and *B. rapa* than *B.*

550 *oleracea*. This might suggest that the prediction of Morales *et al*. (2018), based on careful

551 reconstruction of photosynthetic regulation in Arabidopsis, that persistent stomatal limitation

552 should be observed during longer light flecks, is not general across close crop relatives. There

553 is evidence for considerable variation among plants, including different functional types, in

554 the extent of stomatal limitation during induction (Deans, Brodribb, Busch & Farquhar

555 2019b; McAusland *et al.* 2016). Intraspecific studies addressing crops have also confirmed

556 that the importance of stomatal limitations during induction can differ between species:

557 stomata have little apparent importance in determining genetic variation for induction in

558 soybean or rice (Acevedo-Siaca *et al*. 2020; Soleh *et al.* 2016), but are a dominant factor in

559 cassava (De Souza *et al*. 2020).

561   To evaluate dynamic changes in $V_{c,max}$ and Rubisco limitation *in planta* requires dynamic A/c_i

562   response measurements (Chazdon & Pearcy 1986; Salter et al., 2019; Soleh *et al.* 2016;

563   Taylor & Long 2017). To avoid the potential caveat of $[CO_2]$ effects on half times for

564   photosynthetic induction (Kaiser *et al.* 2017; Woodrow *et al.* 1996), the new dynamic A/c_i

565   protocol used here varied $[CO_2]$ during every induction. This increased the interval between

566   measurements to 2 min compared with 10 s in previous studies (Salter *et al.* 2019; Soleh *et*

567   *al.* 2016; Taylor & Long 2017), so half times for apparent $V_{c,max}$ based on exponential curve

568   fitting (Salter *et al.* 2019; Taylor & Long 2017) were less reliable and we analysed time

569   series using GAMM. Though more qualitative, this analysis provided evidence that increases

570   in apparent $V_{c,max}$ of *B. napus* are sustained over longer periods than in the other two; it

571   augmented the traditional perspective of a two-phase RuBP regeneration and Rubisco

572   activation limited sequence (Pearcy *et al.* 1996) by providing evidence for transitions to co-

573   limitation by *J* after ~ 10 min of induction in *B. napus* and *B. rapa*; and it correctly

574   reproduced limitation-states observed in steady-state measurements 20 min into induction.

575   As with induction experiments, recovery of apparent $V_{c,max}$ was evaluated following

576   shade treatments consistent with expectations for field crops (Burgess *et al.* 2016; Townsend

577   *et al.* 2018; Zhu, Ort, Whitmarsh & Long 2004). The relatively high PPFD used to simulate

578   shade may explain the smaller increases in $V_{c,max}$ (23-33% compared with > ~ 40%) than

579   were observed in sun-shade-sun experiments with wheat (Salter *et al.* 2019; Taylor & Long

580   2017). Timescales for increases in apparent $V_{c,max}$ were, however, consistent with those of

581   wheat, i.e., saturating after 10-15 min induction. That apparent $V_{c,max}$ continued to increase

582   after $t_{ci,min}$ agrees with results from both dynamic A/c_i (Chazdon & Pearcy 1986) and A^* (c_i-

583   corrected *A*, Woodrow & Mott 1989) methods used to establish the duration and impacts of

584   slow-phase limitations. Our results therefore validate the use of those values to model

585   impacts of Rubisco activation during induction (Morales *et al*. 2018; Wang *et al*. 2020).

586   As c_i increased during induction, after ~ 10 min it began to coincide with and exceed

587    $c_{i,trans}$ of both *B. napus* and *B. rapa*. This experimental outcome has important consequences

588   for both the simplified A^* approach to evaluation of biochemical limitations (Woodrow &

589   Mott 1989; Hammond *et al*. 1998) and a recent method incorporating more detailed models

590   of leaf gas exchange to quantify stomatal limitation based on more realistic assumptions

591   about the shape of the A/c_i response (Deans *et al*. 2019a). Both methods assume Rubisco

592   limitation, and our results suggest this is valid in broad terms, but the methods will suffer

593   from reduced accuracy if and when c_i approaches $c_{i,trans}$, because $c_{i,trans}$ marks an inflection in

594   the response of A to c_i.

595   Persistent $V_{c,max}$ limitation in *B. oleracea* meant that A continued to respond to

596   changes in both $V_{c,max}$ and g_s even after 20 min induction. By contrast, transitions to co-

597   limitation by J after ~ 10 min induction in *B. napus* and *B. rapa*, meant A subsequently

598   showed decreased sensitivity to changing V_{cmax} and g_s. *B napus* and *B. rapa* therefore

599   overcame the effects of shade on A more rapidly. Because $c_{i,trans}$ marks an inflection in the

600   response of A to g_s, it has been argued that steady-state operating points in the vicinity of

601    $c_{i,trans}$ can encompass a wide range of values for the marginal cost of water use ($\delta E/\delta A$; von

602   Caemmerer & Farquhar 1981; Farquhar & Sharkey 1982), compatible with a range of

603   alternative water use strategies (Cowan & Farquhar, 1977; Cowan, 1982). An alternative

604   view might be that operation close to $c_{i,trans}$, as observed for *B. napus* and *B. rapa*, results in

605   more rapid declines in A/g_{sw} (intrinsic water use efficiency) during induction, compared with

606    $c_i < c_{i,trans}$, i.e., persistent Rubisco limitation as in *B. oleracea*. Do faster photosynthetic

607   responses to shade among crop plants trade-off against regulation of leaf water status?

608   Further characterisation of the temporal characteristics and/or frequency of deviations

609   between c_i and $c_{i,trans}$ using dynamic A/c_i might provide useful insights into trade-offs between

610   optimisation of radiation and water use efficiencies.

611   *Conclusions*

612   Measurements of three agriculturally important *Brassica* showed that in addition to classic

613   fast RuBP regeneration and slow $V_{c,max}$ limited phases, transitions to co-limitation by J affect

614   the dynamics of photosynthesis following shade. In leaves where c_i approached $c_{i,trans}$ more

615   quickly during induction, subsequent photosynthesis was less sensitive to ongoing changes in

616    $V_{c,max}$ and g_s. Diurnal productivity of C$_3$ crops with lower $c_{i,trans}$ would therefore be expected

617   to be less sensitive to shade. Finally, although only one genotype of each crop was examined,

618   these crops can be interbred, and the variation identified here shows scope for physiologically

619   guided breeding to achieve improved photosynthetic efficiency.

629   **Data availability statement**

630   Data for leaf biochemistry, steady state responses to PPFD and CO_2, induction responses and

631   dynamic A/c_i responses, are available at https://doi.org/10.17635/lancaster/researchdata/378

632

633 **References**

634 Acevedo-Siaca L.G., Coe R., Wang Y., Kromdijk J., Quick W.P. & Long S.P. (2020)

635   Variation in photosynthetic induction between rice accessions and its potential for

636   improving productivity. *New Phytologist* https://doi.org/10.1111/nph.16454.

637 Bradford M.M. (1976) A rapid and sensitive method for the quantitation of microgram

638   quantities of protein utilizing the principle of protein-dye binding. *Analytical*

639   *Biochemistry* **72,** 248–254.

640 Burgess AJ., Retkute R., Preston S.P., Jensen O.E., Pound M.P., Pridmore T.P., & Murchie

641   E.H. (2016) The 4-dimensional plant: Effects of wind-induced canopy movement on

642   light fluctuations and photosynthesis. *Frontiers in Plant Science*, **7,** 1–12.

643 von Caemmerer S. & Farquhar G.D. (1981) Some relationships between the biochemistry of

644   photosynthesis and the gas exchange of leaves. *Planta* **153**, 376–387.

645 von Caemmerer S. & Edmondson D. (1986). Relationship between steady-state gas

646   exchange, *in vivo* Ribulose Bisphosphate Carboxylase activity and some carbon

647   reduction cycle intermediates in *Raphanus sativu*s. *Australian Journal of*

648   *PlantPhysiology*, ***13*,** 669-688.

649 Carmo-Silva A.E. & Salvucci M.E. (2013) The regulatory properties of Rubisco Activase

650   differ among species and affect photosynthetic induction during light transitions. *Plant*

651   *Physiology* **161**, 1645–1655.

652 Carmo-Silva E., Andralojc P.J., Scales J.C., Driever S.M., Mead A., Lawson T., … Parry

653   M.A.J. (2017) Phenotyping of field-grown wheat in the UK highlights contribution of

654   light response of photosynthesis and flag leaf longevity to grain yield. *Journal of*

655   *Experimental Botany* **68**, 3473–3486.

656 Chazdon R.L. & Pearcy R.W. (1986) Photosynthetic responses to light variation in rainforest

657   species I. Induction under constant and fluctuating light conditions. *Oecologia* **69**, 524–

658   531.

659 Cowan I.R. (1982) Regulation of water use in relation to carbon gain in higher plants. In

660   *Encyclopedia of Plant Physiology New Series Volume 12 B*. (eds O.L. Lange, P.S.

661   Nobel, C.B. Osmond & H. Ziegler), pp. 589–614. Springer Verlag, Berlin, Heidelberg,

662   New York.

663 Cowan I.R. & Farquhar G.D. (1977) Stomatal function in relation to leaf metabolism and

664   environment. In *Symposia of the Society for Experimental Biology*. pp. 471–505.

665 Deans R.M., Farquhar G.D. & Busch F.A. (2019a) Estimating stomatal and biochemical

666   limitations during photosynthetic induction. *Plant, Cell & Environment*, **42,** 3227-3240.

667 Deans R.M., Brodribb T.J., Busch F.A. & Farquhar G.D. (2019b) Plant water-use strategy

668   mediates stomatal effects on the light induction of photosynthesis. *New Phytologist* **222**,

669   382–395.

670 Farquhar G.D., von Caemmerer S. & Berry J.A. (1980) A Biochemical Model of

671   Photosynthetic CO_2 Assimilation in Leaves of C_3 Species. *Planta* **149**, 78–90.

672 Farquhar G.D. & Sharkey T.D. (1982) Stomatal Conductance and Photosynthesis. *Annual*

673   *Review of Plant Physiology* **33**, 317–345.

674 Fowler D., Coyle M., Skiba U., Sutton M.A., Cape J.N, Reis S., … Voss M. (2013) The

675   global nitrogen cycle in the twenty-first century. Philosophical Transactions of the Royal

676   Society B **368,** 20130164.

677 Glowacka K., Kromdijk J., Kucera K., Xie J., Cavanagh A.P., Leonelli L., … Long S.P.

678   (2018) Photosystem II Subunit S overexpression increases the efficiency of water use in

679   a field-grown crop. *Nature Communications* **9,** article number 868.

680 Gu L., Pallardy S.G., Tu K., Law B.E. & Wullschleger S.D. (2010) Reliable estimation of

681   biochemical parameters from C_3 leaf photosynthesis-intercellular carbon dioxide

682   response curves. *Plant, Cell and Environment* **33**, 1852–1874.

683 Haddeland I., Heinke J., Biemans H., Eisner S., Florke M., Hanasaki N., … Wisser D. (2014)

684   Global water resources affected by human interventions and climate change.

685   *Proceedings of the National Academy of Sciences of the United States of America* **111**,

686   3251-3256.

687 Hammond E.T., John Andrews T., Mott K.A. & Woodrow I.E. (1998) Regulation of Rubisco

688   activation in antisense plants of tobacco containing reduced levels of Rubisco activase.

689   *Plant Journal* **14**, 101–110.

690 Hanson D.T., Stutz S.S. & Boyer J.S. (2016). Why small fluxes matter: The case and

691   approaches for improving measurements of photosynthesis and (photo)respiration.

692   *Journal of Experimental Botany*, **67,** 3027–3039.

693 Hermida-Carrera, C., Kapralov, M. V, & Galmés, J. (2016). Rubisco catalytic properties and

694   temperature response in crops. *Plant Physiology*, *171*(August), pp.01846.2016

695 Hikosaka K. & Terashima I. (1995) A model of the acclimation of photosynthesis in the

696   leaves of C_3 plants to sun and shade with respect to nitrogen use. *Plant, Cell &*

697   *Environment* **18,** 605–618.

698 Inaba R. & Nishio T. (2002) Phylogenetic analysis of Brassiceae based on the nucleotide

699   sequences of the S-locus related gene, SLR1. *Theoretical and Applied Genetics* **105**,

700   1159–1165.

701 Indermühle A., Stocker T.F., Joos F., Fischer H., Smith H.J., Wahlen M., … Stauffer B.

702   (1999) Holocene carbon-cycle dynamics based on CO_2 trapped in ice at Taylor Dome,

703   Antarctica. *Nature* **398,** 121–126.

704 Kaiser E., Morales A., Harbinson J., Kromdijk J., Heuvelink E. & Marcelis L.F.M. (2015)

705 Dynamic photosynthesis in different environmental conditions. *Journal of Experimental*

706 *Botany* **66**, 2415–2426.

707 Kaiser E., Morales A., Harbinson J., Heuvelink E., Prinzenberg A.E. & Marcelis L.F.M.

708 (2016) Metabolic and diffusional limitations of photosynthesis in fluctuating irradiance

709 in *Arabidopsis thaliana*. *Scientific Reports* **6,** 31252.

710 Kaiser E., Kromdijk J., Harbinson J., Heuvelink E. & Marcelis L.F.M. (2017) Photosynthetic

711 induction and its diffusional, carboxylation and electron transport processes as affected

712 by CO_2 partial pressure, temperature, air humidity and blue irradiance. *Annals of Botany*

713 **119**, 191–205.

714 Kirschbaum M.U.F. & Pearcy R.W. (1988) Gas exchange analysis of the relative importance

715 of stomatal and biochemical factors in photosynthetic induction in *Alocasia*

716 *macrorrhiza*. *Plant Physiology* **86,** 782–785.

717 Kromdijk J, Glowacka K, Leonelli L, Gabilly ST, Iwai M, Niyogi KK, Long SP (2016)

718 Improving photosynthesis and crop productivity by accelerating recovery from

719 photoprotection. *Science* **354,** 857-861.

720 Kromdijk J. & Long S.P. (2016) One crop breeding cycle from starvation ? How engineering

721 crop photosynthesis for rising CO_2 and temperature could be one important route to

722 alleviation. *Proceedings of the Royal Society B*, ***283*,** 20152578.

723 Larson G., Piperno D.R., Allaby R.G., Purugganan M.D., Andersson L., Arroyo-Kalin M., …

724 Fuller D.Q. (2014) Current perspectives and the future of domestication studies.

725 *Proceedings of the National Academy of Sciences of the United States of America* **111,**

726 6139–6146.

727 Lawson T., & Vialet-Chabrand S. (2019). Speedy stomata, photosynthesis and plant water

728 use efficiency. *New Phytologist*, **221,** 93–98.

729 Liu S., Liu Y., Yang X., Tong C., Edwards D., Parkin I.A.P., … Paterson A.H. (2014) The

730   *Brassica oleracea* genome reveals the asymmetrical evolution of polyploid genomes.

731   *Nature Communications* **5,** 3980.

732 Long, S.P. & Hallgren, J.-E. (1993). Measurement of CO_2 assimilation by plants in the field

733   and the laboratory. In *Photosynthesis and Production in a Changing Environment: a*

734   *field and laboratory manual* (eds D.O. Hall, J.M.O. Scurlock, H.R. Bolhàr-

735   Nordenkampf, R.C. Leegood & S.P. Long), pp. 62–94. Chapman & Hall, London,

736   United Kingdom.

737 Long S.P., Ainsworth E.A., Rogers A. & Ort D.R. (2004) Rising atmospheric carbon dioxide:

738   plants face the future. *Annual Review of Plant Biology*, **55,** 591-628.

739 McAusland L., Vialet-Chabrand S., Davey P., Baker N.R., Brendel O. & Lawson T. (2016)

740   Effects of kinetics of light-induced stomatal responses on photosynthesis and water-use

741   efficiency. *New Phytologist* **211**, 1209–1220.

742 Morales A., Kaiser E., Yin X., Harbinson J., Molenaar J., Driever S.M. & Struik P.C. (2018)

743   Dynamic modelling of limitations on improving leaf CO_2 assimilation under fluctuating

744   irradiance. *Plant Cell and Environment* **41,** 589–604.

745 Mott K.A. & Woodrow I.E. (2000) Modelling the role of Rubisco activase in limiting non-

746   steady-state photosynthesis. *Journal of Experimental Botany* **51**, 399–406.

747 Ort D.R., Merchant S.S., Alric J., Barkan A., Blankenship R.E., Bock R., … Zhu X.G. (2015)

748   Redesigning photosynthesis to sustainably meet global food and bioenergy demand.

749   *Proceedings of the National Academy of Sciences* **112,** 8529–8536.

750 Parkin I.A.P., Gulden S.M., Sharpe A.G., Lukens L., Trick M., Osborn T.C. & Lydiate, D.J.

751   (2005). Segmental structure of the *Brassica napus* genome based on comparative

752   analysis with *Arabidopsis thaliana*. *Genetics* **171,** 765–781.

753   Pearcy R.W., Krall J.P. & Sassenrath-Cole G.F. (1996) Photosynthesis in fluctuating light

754   environments. In *Photosynthesis and the Environment*. (ed N.R. Baker), pp. 321–346.

755   Kluwer Academic Publishers, Netherlands.

756   R Core Team (2018) R: A language and environment for statistical computing.

757   Rakow G. (2004) Species Origin and Economic Importance of *Brassica*. In: Pua E.C.,

758   Douglas C.J. (eds) *Brassica. Biotechnology in Agriculture and Forestry* **54,** 3-12

759   Springer, Berlin, Heidelberg

760   Rana D., Van Den Boogaart T., O'Neill C.M., Hynes L., Bent E., Macpherson L., …

761   Bancroft I. (2004) Conservation of the microstructure of genome segments in *Brassica*

762   *napus* and its diploid relatives. *Plant Journal* **40**, 725–733.

763   Raschke K. (1975) Stomatal action. *Annual Review of Plant Physiology* **26**, 309–340.

764   Sage R.F. (1995) Was low atmospheric CO_2 during the pleistocene a limiting factor for the

765   origin of agriculture. *Global Change Biology,* **1**, 93-106.

766   Salesse-Smith C.E., Sharwood R.E., Busch F.A., Kromdijk J., Bardal V. & Stern D.B. (2018)

767   Overexpression of Rubisco subunits with RAF1 increases Rubisco content in maize.

768   *Nature Plants* **4,** 802-810.

769   Salter W.T., Merchant A.M., Richards R.A., Trethowan R. & Buckley T.N. (2019) Rate of

770   photosynthetic induction in fluctuating light varies widely among genotypes of wheat.

771   *Journal of Experimental Botany* **70**, 2787–2796.

772   Sassenrath-Cole G.F. & Pearcy R.W. (1992) The role of ribulose-1,5-bisphosphate

773   regeneration in the induction requirement of photosynthetic CO_2 exchange under

774   transient light conditions. *Plant Physiology* **99,** 227–234.

775   Sharwood R.E., Sonawane B.V., Ghannoum O. & Whitney S.M. (2016) Improved analysis of

776   C_4 and C_3 photosynthesis via refined *in vitro* assays of their carbon fixation

777   biochemistry. *Journal of Experimental Botany* **67**, 3137–3148.

778 Sharkey T.D., Bernacchi C.J., Farquhar G.D. & Singsaas E.L. (2007) Fitting photosynthetic

779 carbon dioxide response curves for C$_3$ leaves. *Plant, Cell and Environment* **30**, 1035-

780 1040.

781 Soleh M.A., Tanaka Y., Kim S.Y., Huber S.C., Sakoda K. & Shiraiwa T. (2017)

782 Identification of large variation in the photosynthetic induction response among 37

783 soybean [*Glycine max* (L.) Merr.] genotypes that is not correlated with steady-state

784 photosynthetic capacity. *Photosynthesis Research* **131**, 305–315.

785 Soleh M.A., Tanaka Y., Nomoto Y., Iwahashi Y., Nakashima K., Fukuda Y., … Shiraiwa T.

786 (2016) Factors underlying genotypic differences in the induction of photosynthesis in

787 soybean [*Glycine max* (L.) Merr.]. *Plant, Cell & Environment* **39**, 685–693.

788 De Souza A.P., Wang Y., Orr D.J., Carmo-Silva E. & Long S.P. (2020) Photosynthesis

789 across African cassava germplasm is limited by Rubisco and mesophyll conductance at

790 steady state, but by stomatal conductance in fluctuating light. *New Phytologist* **225,**

791 2498-2512.

792 Stephenson P., Baker D., Girin T., Perez A., Amoah S., King G.J. & Østergaard L. (2010) A

793 rich TILLING resource for studying gene function in *Brassica rapa*. *BMC Plant Biology*

794 **10,** 1–10.

795 Tanaka Y., Adachi S. & Yamori W. (2019) Natural genetic variation of the photosynthetic

796 induction response to fluctuating light environment. *Current Opinion in Plant Biology*

797 **49,** 52–59.

798 Taylor S.H. & Long S.P. (2017) Slow induction of photosynthesis on shade-sun transitions in

799 wheat may cost at least 21% of productivity. *Philosophical Transactions of the Royal*

800 *Society B: Biological Sciences* **372**, 20160543.

801   Terashima I., Fujita T., Inoue T., Chow W.S. & Oguchi R. (2009) Green light drives leaf

802   photosynthesis more efficiently than red light in strong white light: revisiting the

803   enigmatic question of why leaves are green. *Plant & Cell Physiology* **50,** 684–697.

804   Tilman D., Balzer C., Hill J. & Befort B.L. (2011) Global food demand and the sustainable

805   intensification of agriculture. *Proceedings of the National Academy of Sciences of the*

806   *United States of America* **108,** 20260–20264.

807   Townsend A.J., Retkute R., Chinnathambi K., Randall J.W.P., Foulkes J., Carmo-Silva E. &

808   Murchie E.H. (2018) Suboptimal acclimation of photosynthesis to light in wheat

809   Canopies. *Plant Physiology* **176**, 1233–1246.

810   Wang Y., Burgess S.J., de Becker E., & Long S.P. (2020). Photosynthesis in the fleeting

811   shadows: An overlooked opportunity for increasing crop productivity? *The Plant*

812   *Journal* **101,** 874–884.

813   Wintermans J.F.G.M. & De Mots A. (1965) Spectrophotometric characteristics of

814   chlorophylls a and b and their phenophytins in ethanol. *Biochimica et Biophysica Acta*

815   *(BBA) - Biophysics including Photosynthesis* **109,** 448–453

816   Woodrow I.E., Kelly M. & Mott K.A. (1996) Limitation of the rate of ribulosebisphosphate

817   carboxylase activation by carbamylation and ribulosebisphosphate carboxylase activase

818   activity: development and tests of a mechanistic model. *Australian Journal of Plant*

819   *Physiology* **23**, 141-149.

820   Woodrow I.E. & Mott K.A. (1989) Rate limitation of non-steady-state photosynthesis by

821   ribulose-1,5-bisphosphate carboxylase in spinach. *Australian Journal of Plant*

822   *Physiology* **16**, 487–500.

823 Yamori W., Masumoto C., Fukayama H. & Makino A. (2012) Rubisco activase is a key

824   regulator of non-steady-state photosynthesis at any leaf temperature and, to a lesser

825   extent, of steady-state photosynthesis at high temperature. *The Plant Journal* **71,** 871–

826   880.

827 Yoon D.-K., Ishiyama K., Suganami M., Tazoe Y., Watanabe M., Imaruoka S., … Makino A.

828   (2020). Transgenic rice overproducing Rubisco exhibits increased yields with improved

829   nitrogen-use efficiency in an experimental paddy field. *Nature Food*, **1,** 134–139.

830 Zhu X.G., Ort D.R., Whitmarsh J. & Long S.P. (2004) The slow reversibility of photosystem

831   II thermal energy dissipation on transfer from high to low light may cause large losses in

832   carbon gain by crop canopies: A theoretical analysis. *Journal of Experimental Botany*

833   **55**, 1167–1175.

834 Zhu X.G., Long S.P. & Ort D.R. (2010) Improving photosynthetic efficiency for greater

835   yield. *Annual Review of Plant Biology* **61,** 235–61.

836 Zuur A.F., Ieno E.N., Walker N.J., Saveliev A.A. & G M Smith (2009) *Mixed Effects Models*

837   *and Extensions in Ecology with R*. (eds M. Gail, K. Krickeberg, J.M. Samet, A. Tsiatis

838   & W Wong), Springer, New York.

839

840 **Table 1** Rubisco amount, specific and total activity for three *Brassica* (mean ± SEM, N = 5).

Species	Rubisco total activity (μmol m^{-2} s^{-1})	Rubisco amount (g m^{-2})	Rubisco specific activity (μmol g^{-1} s^{-1})	Total soluble protein (g m^{-2})	Chlorophylls a and b (g m^{-2})	Chlorophyll a:b
B. oleracea	38 ± 4.0	1.61 ± 0.322	25.5 ± 2.37	3.88 ± 0.218[a]	0.500 ± 0.025[a]	2.14 ± 0.051[a]
B. napus	46 ± 3.6	1.79 ± 0.147	26.1 ± 0.86	4.83 ± 0.266[b]	0.428 ± 0.025[a]	2.28 ± 0.02[ab]
B. rapa	48 ± 4.9	1.87 ± 0.23	25.7 ± 0.62	3.77 ± 0.185[a]	0.290 ± 0.014[b]	2.42 ± 0.049[b]

841 Different superscripts indicate significant differences at P < 0.05 using Tukey's HSD.

842 **Table 2** Steady-state values for leaf net CO_2 assimilation (A), stomatal conductance to H_2O

843 (g_{sw}), intrinsic water use efficiency (iWUE = A/g_{sw}), intercellular [CO_2] (c_i), c_i for the

844 limitation-state transition from $V_{c,max}$ to J ($c_{i,trans}$), and stomatal limitation (L$_S$) of three

845 *Brassica*, at: PPFD, 1500 μmol m^{-2} s^{-1}; leaf temperature, 25 °C; and leaf-air vapour pressure

846 deficit, 1.2 kPa, and $CO_2 \sim 400$ μmol mol^{-1} (mean ± SEM, N = 4).

Species	A (μmol m^{-2} s^{-1})	g_{sw} (mol m^{-2} s^{-1})	c_i (Pa)	$c_{i,trans}$ (Pa)	L$_S$ (%)
B. oleracea	32.5 ± 0.69[a]	0.46 ± 0.055[a]	26.5 ± 0.95	35.1 ± 1.55[a]	21.9 ± 2.24[a]
B. napus	36.6 ± 1.67[ab]	0.63 ± 0.040[ab]	28.3 ± 0.40	31.6 ± 2.07[ab]	14.5 ± 1.98[ab]
B. rapa	37.7 ± 0.44[b]	0.75 ± 0.071[b]	29.3 ± 1.04	28.8 ± 0.7[b]	12.8 ± 2.21[b]

847 Different superscripts indicate significant differences at P < 0.05 using Tukey's HSD.

848   **Table 3** Statistical summary of photosynthetic induction characteristics in three *Brassica*.

849   Mean ± SEM (N = 3, *B. oleracea*; N = 4, *B. napus & B. rapa*).

Species	B. oleracea	B. napus	B. rapa
Recovery in A at end of fast phase: two minutes after shade (R_{fast}, %)	64 ± 4.9	72 ± 4.8	72 ± 3.2
Recovery in A, at c_i minimum ($R_{ci,min}$, %)	77 ± 5.0	81 ± 3.7	84 ± 3.5
Slow phase recovery ($R_{ci,min} - R_{fast}$, %)	12.6 ± 0.77	10 ± 2.41	11.8 ± 1.81
Time to c_i minimum* ($t_{ci,min}$, min)	5.2 ± 0.59	4.1 ± 0.34	4.6 ± 0.34
Time to 90% recovery of A ($t_{A,90}$, min)	16.7 ± 3.49[a]	8.7 ± 2.02[b]	7.4 ± 1.41[b]
Duration of recovery associated with increasing c_i ($t_{A,90} - t_{ci,min}$, min)	11.5 ± 3.28[a]	4.6 ± 1.71[ab]	2.75 ± 2.2[b]

850   Different superscripts indicate differences with P < 0.1 using Tukey's HSD.

39

Figure Captions

Fig. 1 Responses of photosynthesis to light, for three *Brassica* species: (a) *B. oleracea*; (b) *B. napus*; (c) *B. rapa*. Non-rectangular hyperbola parameters: effective quantum yield (ϕ), asymptotic gross CO_2 assimilation rate (A_{sat}), curvature (θ), and day respiration (R_d) are provided as mean $\pm$ SEM (N=4) across models fit to independent replicates within each species. Lines represent combined parameter means, and two representative sets of data are shown.

Fig. 2 CO_2 response curves show that shifts in operating c_i, and the c_i at which the factor limiting net CO_2 assimilation rate transitions from $V_{c,max}$ to J, result in different biochemical limitations of steady state photosynthesis among three *Brassica* species: (a) *B. oleracea* (circles); (b) *B. napus* (diamonds); (c) *B. rapa* (triangles). Maximum net CO_2 assimilation rates attributable to carboxylation limited by Rubisco (A_C), electron transport (A_J), and triose phosphate utilisation (A_P); CO_2 compensation point (Γ); and c_i values marking transitions between biochemical limiting factors, are plotted relative to mean operating points (grey fill, SEM smaller than symbol size). Also shown, are mean $\pm$ SEM (N=4) for maximum Rubisco limited carboxylation rate ($V_{c,max}$), electron transport rate (J), and triose phosphate utilisation (T_P). Shading distinguishes two example data sets per species. Models were fit to data for individual leaves before summarizing parameters.

Fig. 3 Induction of net CO_2 assimilation (A), stomatal conductance (g_{sw}), and intercellular CO_2 (c_i) for three *Brassica* species, responding to an abrupt shift in photosynthetic photon flux density (PPFD), to 1500 µmol m^{-2} s^{-1} after 30 minutes at 150 µmol m^{-2} s^{-1}. Mean $\pm$ SEM for (a) *B. oleracea* (N=3), (b) *B. napus* (N=4), (c) *B. rapa* (N=4). Dashed lines indicate steady state values obtained at 1500 µmol m^{-2} s^{-1} PPFD prior to shade.
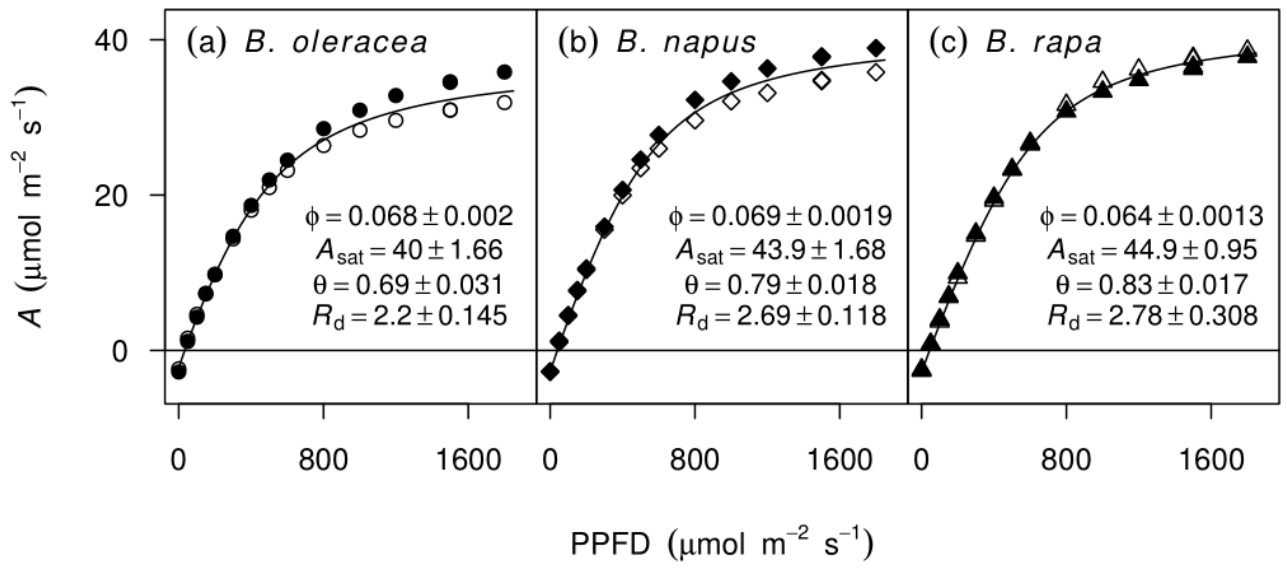
876   **Fig. 4** Time dependence of $V_{c,max}$ (a-c) and $dV_{c,max}/dt$ (d) following induction for (a) *Brassica*

877   *oleracea* (N = 4), (b) *B. napus* (N = 4), and (c) *B. rapa* (N = 3). Arrows indicate mean

878   values for the time to recover 90% of A, measured in separate induction measurements at

879   ambient [CO_2] ($t_{A,90}$; Table 3).

880

881   **Fig. 5** Post-shade response of transition c_i values ($c_{i,trans}$), at which biochemical limitation

882   switches from maximum rate of carboxylation by Rubisco ($V_{c,max}$) to either rate of electron

883   transport (A_C/A_J, open symbols) or triose phosphate limitation (A_C/A_P, closed symbols), and c_i

884   measured during induction at ambient [CO_2] (small grey symbols, see also Fig. 3). Where $c_i <$

885     $c_{i,trans}$ supports $V_{c,max}$ limitation, and $c_i > c_{i,trans}$ limitation by factors other than $V_{c,max}$. (a)

886   *Brassica oleracea* (N = 4), (b) *B. napus* (N = 4), and (c) *B. rapa* (N = 3). Steady-state $c_{i,trans}$

887   (dashed lines; Table 2), and time to recover 90% of A, measured in separate induction

888   measurements at ambient [CO_2] (arrows, $t_{A,90}$; Table 3), are shown for reference.

889

Fig. 1

(a) *B. oleracea*

$\phi = 0.068 \pm 0.002$
$A_{sat} = 40 \pm 1.66$
$\theta = 0.69 \pm 0.031$
$R_d = 2.2 \pm 0.145$

(b) *B. napus*

$\phi = 0.069 \pm 0.0019$
$A_{sat} = 43.9 \pm 1.68$
$\theta = 0.79 \pm 0.018$
$R_d = 2.69 \pm 0.118$

(c) *B. rapa*

$\phi = 0.064 \pm 0.0013$
$A_{sat} = 44.9 \pm 0.95$
$\theta = 0.83 \pm 0.017$
$R_d = 2.78 \pm 0.308$

A (μmol m^{-2} s^{-1})

PPFD (μmol m^{-2} s^{-1})

Fig. 2

(a) *B. oleracea*

A_C
A_J
A_P

$V_{c,max} = 127 \pm 1.3$
$J = 221 \pm 5.2$
$T_P = 15.8 \pm 0.38$

(b) *B. napus*

$V_{c,max} = 138 \pm 9.7$
$J = 228 \pm 8.9$
$T_P = 15.7 \pm 0.54$

(c) *B. rapa*

$V_{c,max} = 145 \pm 4.6$
$J = 231 \pm 7.7$
$T_P = 16.3 \pm 0.82$

A (μmol m^{-2} s^{-1})

c_i (Pa)

893

Fig. 3

Fig. 4

time since shade (min)

Fig. 5

(a) *B. oleracea*

(b) *B. napus*

(c) *B. rapa*

c_i (Pa)

time since shade (min)

$t_{A,90}$